LAWRENCE
LIVERMORE
NATIONAL
LABORATORY

UCRL-CONF-217871

Spinodal Ordering and Precipitation in U-6 wt% Nb

Luke Hsiung, Jikou Zhou

December 22, 2005

2005 MRS Fall Meeting
Boston, MA, United States
November 28, 2005 through December 2, 2005

SPINODAL ORDERING AND PRECIPITATION IN U-6 wt% Nb

Luke Hsiung and Jikou Zhou

Lawrence Livermore National Laboratory
Chemistry and Materials Science Directorate
P.O. Box 808, L-352
Livermore, CA 94551-9900

Abstract--A combinative approach of microhardness testing, tensile testing, and TEM microstructural analysis was employed to study the microstructure and mechanical instability of a water-quenched U-6wt.% Nb (WQ-U6Nb) alloy subjected to different aging schedules including artificial aging at 200°C, 15-year natural aging at ambient temperatures, and 15-year natural aging followed by accelerative aging at 200°C. The changes in mechanical property during and after the aging processes were examined using microhardness and tensile-testing methods. During the early stages of artificial aging at 200°C, the microhardness of WQ-U6Nb alloy increased, i.e., age hardening, as a result of the development of nanoscale modulation caused by spinodal decomposition. Coarsening of the modulated structure occurred after a prolonged aging at 200°C for 16 hours, and it led to a decrease of microhardness, i.e., age softening. Phase instability was also found to occur in WQ-U6Nb alloy that was subjected to a 15-year natural aging at ambient temperatures. The formation of partially ordered domains resulting from a spinodal modulation with an atomic-scale wavelength rendered the appearance of swirl-shape antiphase domain boundaries (APBs) observed in TEM images. Although it did not cause a significant change in microhardness, 15-year natural aging has dramatically affected the aging mechanisms of the alloy isothermally aged at 200°C. Microhardness values of the NA alloy continuously increased after isothermal aging at 200°C for 96 hours as a result of the phase decomposition of partially ordered domains into Nb-depleted α phase and Nb-enriched U_3Nb ordered phase in the alloy. It is concluded that the long-term natural aging changes the transformation pathway of WQ-U6Nb, and it leads to order-disorder transformation and precipitation hardening of WQ-U6Nb alloy.

Introduction

It is well known that U-6wt. %Nb (U-14 at. %Nb) alloy as exploited for a variety of engineering applications has a microstructure containing martensitic phases supersaturated with Nb, which can be obtained by rapid quenching the alloy from γ (bcc)-field solid solution to room temperature [1, 2]. The high cooling rate forces the γ-phase solid solution to transform martensitically to a variant of the low temperature α (orthorhombic) phase in which Nb is retained in supersaturated solid solution. Because the variant phase is supersaturated and its lattice parameters differ from the equilibrium α phase, it has been designated α' martensite. Two additional variant phases, a monoclinic distortion of α', named α'' martensite, or a tetragonal distortion of γ, named γ^o martensite, can also be formed within the as-quenched material. The resulting alloy has improved mechanical properties (ductility and toughness) and excellent corrosion resistance because of the uniform distribution of Nb in solid solution that suppresses the diffusional decomposition reaction to form two-phase (an α phase and a Nb-enriched γ phase) cellular microstructures, which are undesirable for engineering applications.

It has been reported that the water-quenched (WQ) U6Nb alloy containing extensively twinned α'' martensitic microstructure results in low yield strength (~200 MPa) and high tensile ductility (~30%) [2]. It has also been demonstrated that the U-Nb alloy containing α'' martensite reveals shape memory effect [3], and the shape memory behavior is controlled mainly by the twin structures within the alloy [4]. Aging of the α'' martensite in the 150°C to 400°C range results in an increase of yield strength to as high as 1.3 GPa due to very fine scale microstructural changes [5], which have not yet been fully characterized but may have involved spinodal decomposition. Over-aging occurs at temperatures above 400°C, where cellular decomposition occurs to form coarse two-phase cellular microstructures. The occurrence of these decompositions in association with Nb segregation can subsequently deteriorate and embrittle the alloy by reducing ductility and toughness as well as corrosion resistance [2, 5]. Therefore, it is necessary to investigate and understand the aging effects on the

microstructural and phase stability of WQ-U6Nb alloy. The investigation of aging effects on WQ-U6Nb reported in the open literature up to present has mainly been placed on aging at temperatures above 400°C, relatively little is known about the aging mechanism of WQ-U6Nb below 400°C. A detailed investigation of segregation reaction within isothermally aged WQ-U6Nb below 400°C was previously reported by Beverini and Edmonds [6], who investigated the low-temperature aging behavior using Vickers hardness measurement and Atom Probe Field Ion Microscopy (APFIM) methods. According to their report, an age hardening/softening phenomenon associated with nanometer length-scale of segregation reaction, possibly spinodal decomposition, was detected within the aged alloy samples. It is noted that the spinodal decomposition is a continuous clustering mechanism in which the supersaturated solid solution separates spontaneously into solute-lean and solute-rich phases within the parent phase domain through uphill diffusion, which is totally different from the nucleation and growth mechanism via downhill diffusion [7]. In order to further elucidate the low-temperature aging mechanisms, our investigation was accordingly focused on the phase stability of the WQ-U6Nb alloy during isothermal aging below 200°C.

Experimental procedure

The U6Nb alloy used for this investigation was wrought processed from Rocky Flats VAR VAR ingot at the BWXT/Bechtel Y-12 plant. Detailed information regarding the fabrication process can be found in Ref. [2]. The naturally aged specimens were machined directly from a 38 mm thick plate. Rod-shaped specimens of 3 mm in diameter were prepared for microstructure analysis and artificial aging experiments. The water-quenched U6Nb alloy was obtained by solution treating the alloy at 800°C for 4 hours followed by water quenching. It was then followed by artificially aging. The artificial aging experiments were carried out in a vacuum furnace at 200°C. The naturally aged (NA) samples used for this investigation were prepared from a 15-year old mechanical part. Microhardness measurements were performed on all these samples using a Vickers-hardness indenter. This was done to monitor the mechanical property change during aging processes. The applied load was 50 g and the time duration is 35 seconds for each test. To obtain a statistically significant value, more than six tests were conducted for each measurement. The microstructures of the alloy in as water-quenched (WQ), WQ plus artificial age (AA), WQ plus natural age (NA), and WQ plus NA and AA (specified as accelerative aging hereafter) conditions were examined using a JEOL-200CX transmission electron microscope (TEM). TEM foils were machined from the rod-shape samples, and the final thinning of the foils was prepared by twin-jet electropolishing in a solution of 45 vol% methanol, 45 vol% butyl alcohol, and 10 vol% nitric acid at 50 V and –20°C.

Results and Discussion

Artificial aging of WQ alloy at 200 °C

The changing of microhardness of WQ-U6Nb with increasing time of artificial aging at 200°C is presented in Fig. 1. Here, the changing of microhardness measured from the accelerative aging of NA samples is also shown in Fig. 1 for a comparison. The alloy in water-quenched condition had an average microhardness of 190.0. It rapidly increased to 210.0 after aging for 2 hours. The microhardness values increased to 237.0 for 4 hours and 254.8 for 8 hours. Within the first 8 hours of aging, the strengthening continued but with a decreasing trend. Further aging caused softening after the microhardness reaches a maximum value at 8 hours, and the microhardness reduced to 237 at 16 hours. No significant change on TEM morphology was found in the low-magnification images shown in Fig. 2. However, modulated microstructures were observed in high-magnification images shown in Fig. 3. The modulated structure contains very fine domains with thickness of ~3 nm, which was attributed to the formation of Nb-lean and Nb-rich phases. The modulated structure was found to initiate at 2 hours, and fully developed between 4 hours and 8 hours. The modulated structure resulted in the formation of satellite spots around the Bragg diffraction spots of the diffraction pattern. These are indicated in the diffraction patterns shown in Figs. 3a -3c. It is worth noting that the dark/bright fringes in TEM image accompanied by the appearance of satellite diffraction spots are typically resulting from spinodal decomposition [8, 9]. For an artificial aging at 200°C, spinodal decomposition initiated and grew within the first 8 hours. After modulation was fully developed, further aging led to the coarsening of the modulated structure. The modulation wavelength increased to ~50 nm after aging for 16 hours, which is shown in Fig. 3d. The microhardness is significantly decreased (Fig. 1) when the coarsening of modulation occurred.

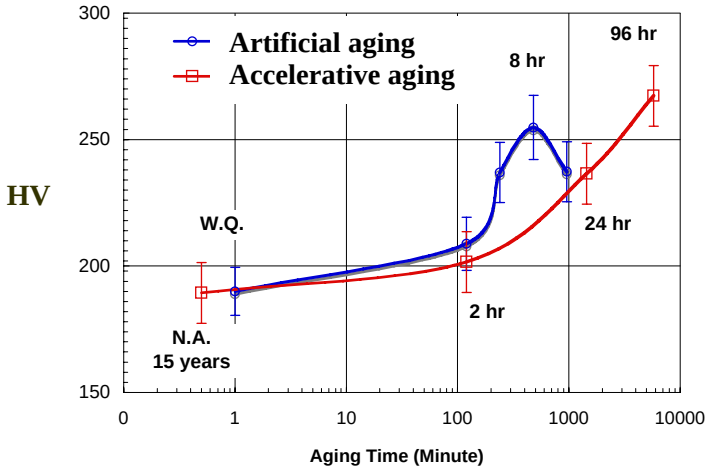

Fig. 1: Changes of microhardness during the artificial aging of WQ-U6Nb alloy and the accelerative aging of 15-year NA-U6Nb alloy.

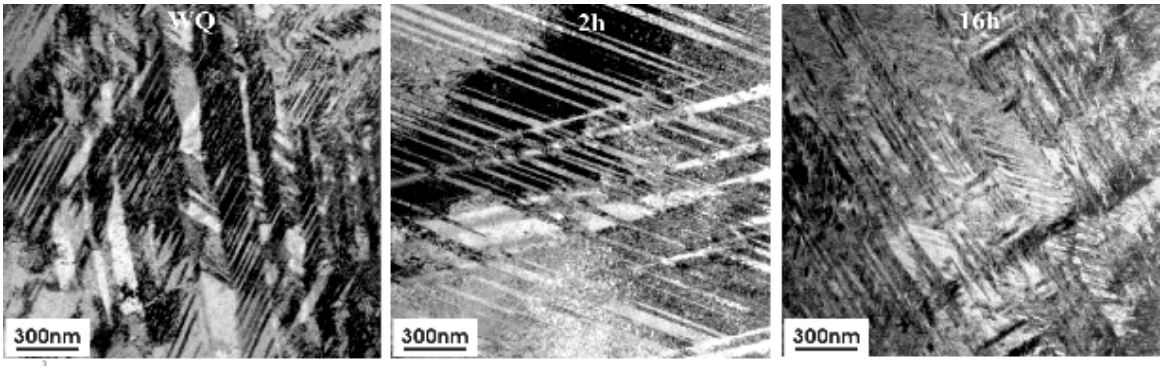

Fig. 2: Low-magnification TEM images showing the microstructure of as water-quenched sample and the microstructures of samples after artificial aging at 200 °C for 2 hours and 16 hours.

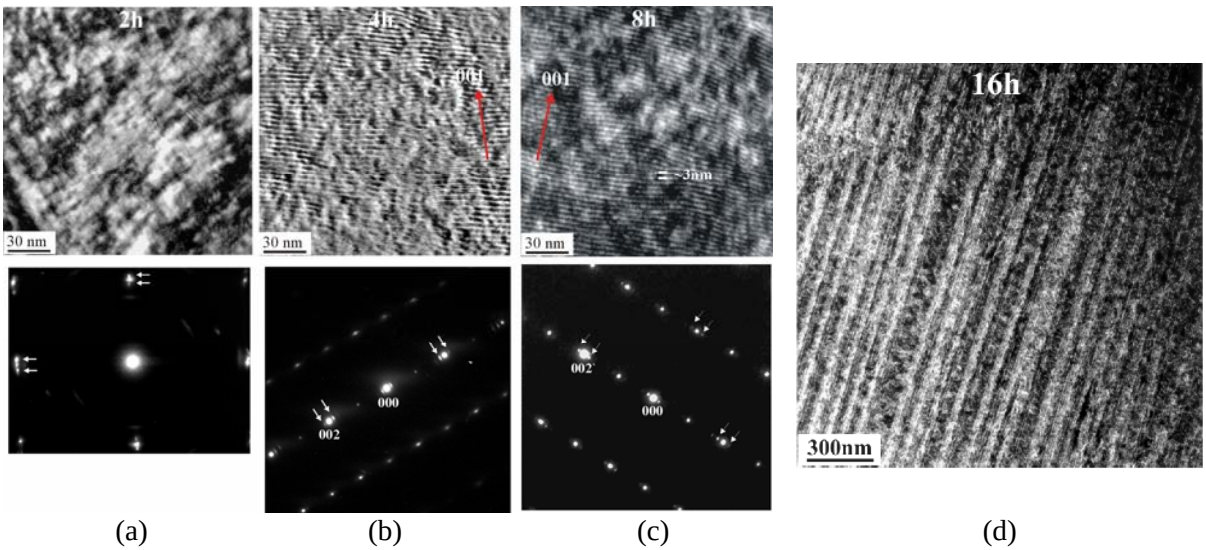

Fig. 3: TEM images and selected-area diffraction (SAD) patterns showing the formation of modulated structures within the artificially aged 2h, 4h, 8h and 16h samples. Satellite (Side) spots caused by the modulation are arrowed in SAD patterns shown in (a), (b), and (c). Coarsening of the modulation observed in 16h sample is shown in (d).

Natural aging at room temperature

Similar to the artificially aged (AA) samples, the change of microstructural morphology within the 15-year NA sample is barely noticeable. However, a very interesting finding within the NA sample is the formation of swirl-shape antiphase domain boundaries (APBs) as shown in Fig. 4. It is worthy to note that the contrast of antiphase domain boundary (also known as π boundary) is visible when the phase angle $\alpha = 2\pi\mathbf{g}\bullet\mathbf{P} = \pi$ and is invisible when $\alpha = 2\pi$ (where **g** is the reflection vector for imaging, and **P** is the displacement vector of APB) [10]. The observation of APBs reveals the occurrence of a disorder-order transformation, which results in the formation of chemically ordered domains within the NA sample. In essence, the ordered phase domain has the same crystal structure as that of the disordered phase domain, except it takes up a superlattice arrangement because of the periodic occupation of lattice sites by specific atom species. Accordingly, new chemically ordered α'' phase is proposed and its structure is identified by a comparison between observed and simulated diffraction patterns. The illustrations of two possible schemes for the disorder-order transformation in α'' phase are illustrated in Fig. 5. For the ordering transformation of Scheme I, U atoms occupy the following three specific lattice sites of the ordered superlattice (4 lattice sites/unit cell): (0,5/6,1/2), (1/2,1/3,1/2), and (1/2,1/2,0), whereas the (0,0,0) lattice site is randomly occupied by U and Nb atoms, in which the probability of the site occupied by U and Nb are 44% and 56%, respectively. For the ordering transformation of Scheme II, U atoms occupy (0,5/6,1/2) and (1/2,1/3,1/2) lattice sites, whereas the (0,0,0) and (1/2,1/2,0) lattice sites are randomly occupied by U and Nb atoms, in which the probability of the sites occupied by U and Nb are 72% and 28%, respectively. The systematic variations in the atomic positions result in different ordered-domains separated by APBs across which the atoms have the wrong immediate neighbors, which is illustrated in Fig. 5(a). It is also noted that the Scheme II ordering transformation as illustrated in Fig. 5(b) may also be considered as a spinodal decomposition with the wave-length (λ) of composition fluctuation that is equal to the lattice parameter of α'' unit cell in the z-direction, i.e. $\lambda = c = 0.495$ nm, which is approximately an order smaller than that observed within samples artificially aged at 200°C.

The [110]-, [310]-, [312]-, and [100]-zone selected-area diffraction patterns generated from the 15-year NA sample are shown in Figs. 6 and 7, in which the corresponding zone diffraction patterns simulated according to the Schemes I and II ordering transformations are also displayed. It is noted that the simulation patterns of the [110]-, [310]-, and [312]-zone are identical between Scheme I and II as shown in Fig. 6, whereas the simulation patterns of the [001]-zone are different between Scheme I and II as shown in Fig. 7. The ordering transformation of α'' phase is identified to be most likely of Scheme II type in accordance to the observed and simulated [100]-zone patterns as shown in Fig. 7. A typical **g•P** image-contrast analysis for APBs in a 15-year NA sample is shown in Fig. 8, where the APBs are visible using $00\bar{1}$ and $0\bar{2}\bar{1}$ superlattice reflections but become invisible when using $0\bar{2}0$ fundamental reflection to image.

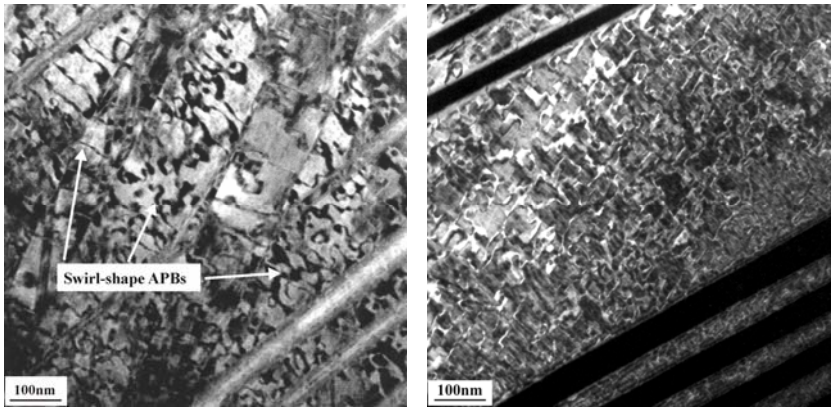

(a) (b)

Fig. 4: Bright-field (a) and dark-field (b) TEM images reveal the formation of swirl-shape antiphase domain boundaries (APBs) within the 15-year NA sample. Notice that APBs appear as a dark contrast in (a) and a bright contrast in (b).

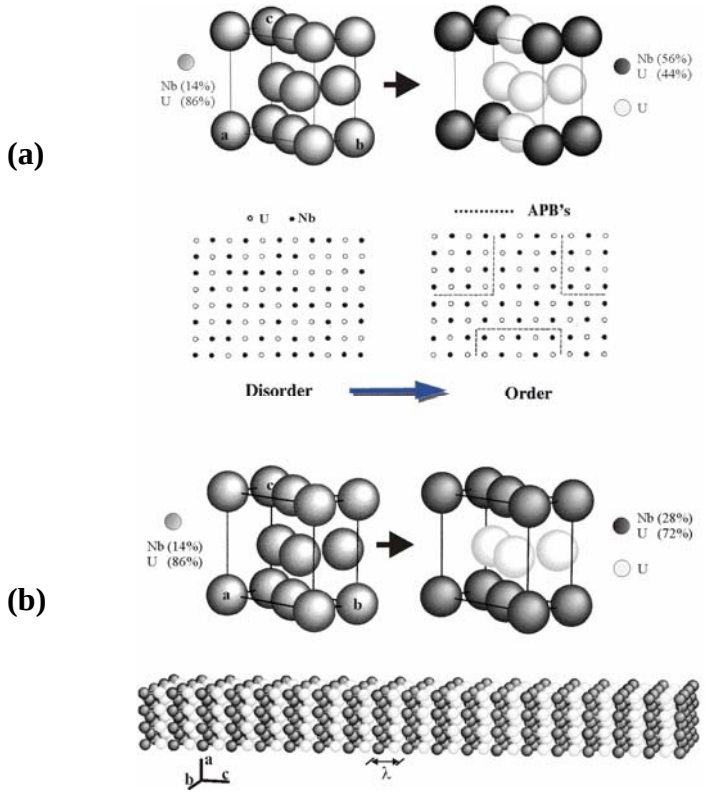

Fig. 5: Schematic illustrations showing two possible schemes proposed for the disorder-order transformation occurred in the binary U-14at%Nb (U-6wt%Nb) alloy, in which two different partially ordered α″ unit cells can be generated according to (a) Scheme I. and (b) Scheme II ordering transformations.

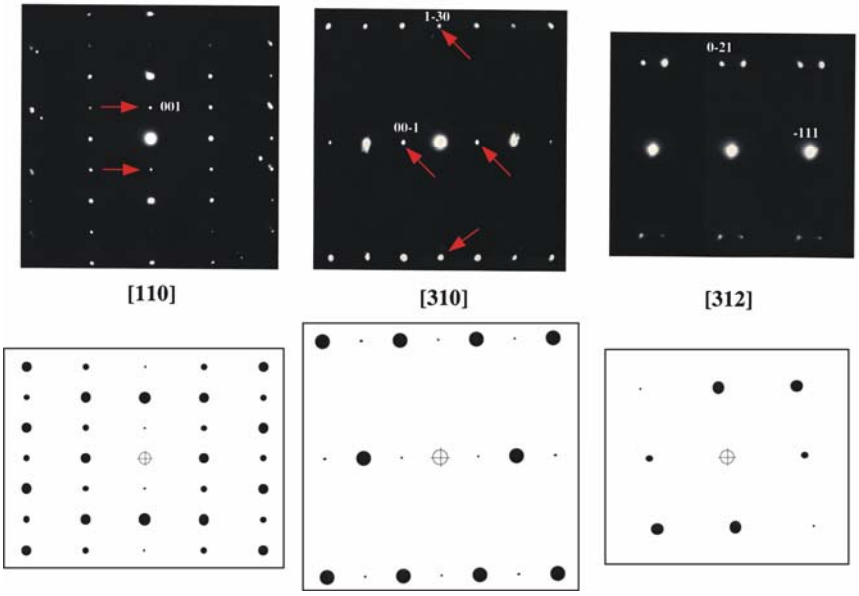

Fig. 6: The [110]-, [310]-, and [312]-zone diffraction patterns generated from the 15-year NA sample, in which the superlattice spots are arrowed (upper). Note that the [312]-zone diffraction pattern includes the diffraction spots generated from twin domains. The corresponding zone diffraction patterns simulated for the proposed ordered α″ unit cell according to Schemes I and II ordering transformations are shown below.

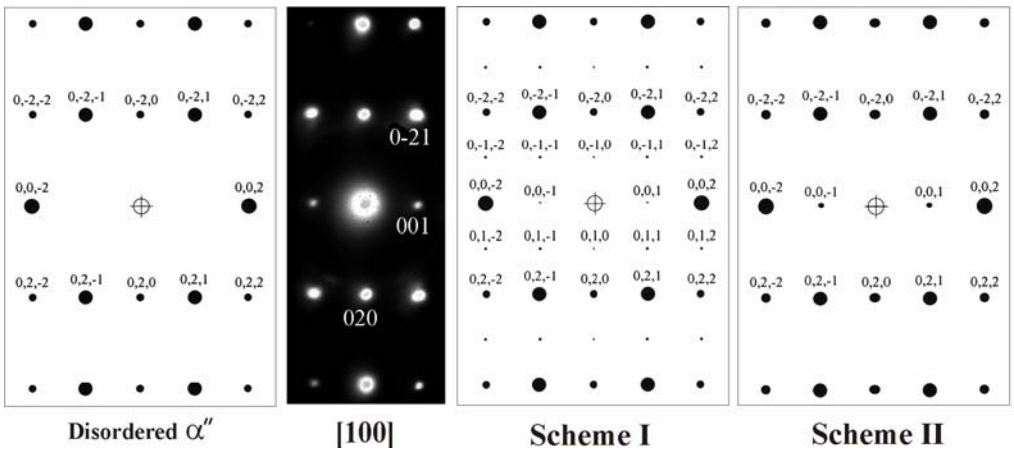

Fig. 7: The [100]-zone diffraction pattern generated from 15-yr NA sample shown with simulated patterns based upon scheme I and scheme II unit cells. Here, scheme II is more likely to be the one for the partially ordered α″ phase according to the comparison between observed and simulated patterns.

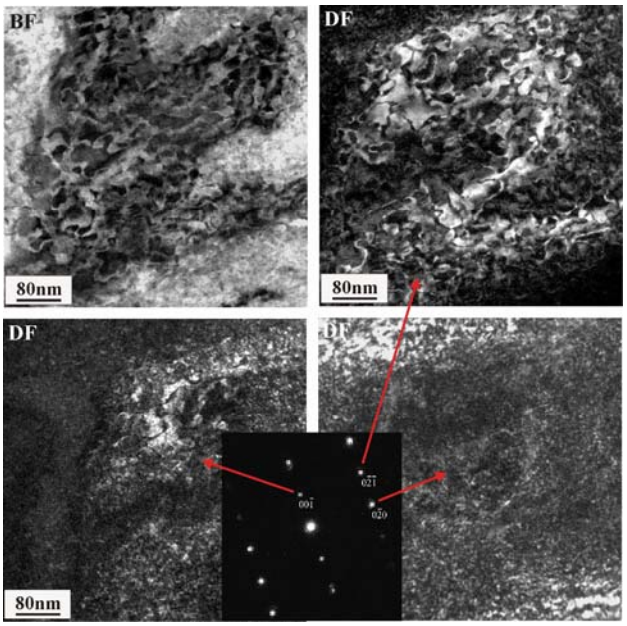

Fig. 8: BF and DF images of growth APBs in an ordered α″ domain observed in the same area. The APBs are visible using $00\bar{1}$ and $0\bar{2}\,\bar{1}$ superlattice reflections but become invisible when using $0\bar{2}0$ fundamental reflection to image.

Accelerative aging of NA alloy at 200 °C

In an effort to study how the long-term natural aging affects the subsequent aging kinetics of the alloy, a 15-year NA alloy sample was isothermally aged at 200°C. The changes of microhardness with increasing aging durations are shown in Fig. 2. Notice that the 15-year NA sample has an initial microhardness value of 189.4, which is very close to that of as water-quenched U6Nb alloy. This suggests that natural aging over the past 15 years does not cause a significant change in mechanical property of the alloy. The microhardness of the alloy slightly increases to 202.6 after aging for 2 hours, and it continuously increases to 236.5 and 267.3 after aging for 24 hours and 96 hours, respectively. It is interesting to note that the NA alloy was not age softened even after it aging for 96 hours, and this is very different from the artificial aging of as water-quenched U6Nb, in which age softening occurred after aging at 200°C for longer than 8 hours. A typical microstructure of NA alloy

isothermally aged at 200°C for 96 hours is shown in Figure 9. Again, there is no significant change observed at low magnifications. Also, there is no modulated structure similar to that shown in Figure 4 was observed at high magnifications. However, the appearance of superlattice diffraction spots in electron diffraction patterns revealed that ordered α″ phase was formed after the NA alloy was isothermally aged for 96 hours at 200°C. Typical selected-area electron diffraction (SAD) patterns of [010]-zone are presented in Fig. 9a. The SAD patterns show readily that a fully ordered U_3Nb phase was formed. It is noted that the two phases identified by comparing the SAD patterns with the simulated diffraction patterns are α and U_3Nb phases. The simulated SAD patterns of [010] zone axis are presented in Fig. 9b. We did not observe the diffraction pattern corresponding to UNb with 50 at.% of Nb, which was observed in the NA specimens.

(a)

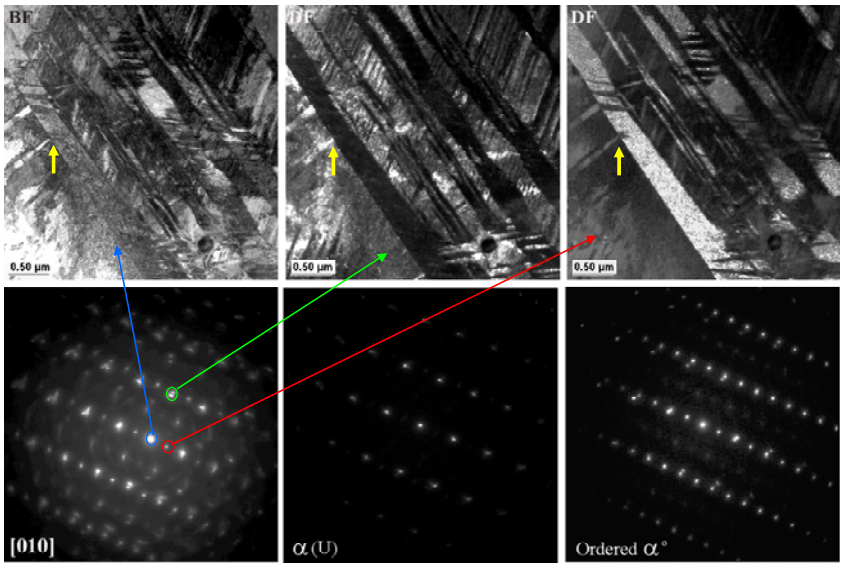

(b)

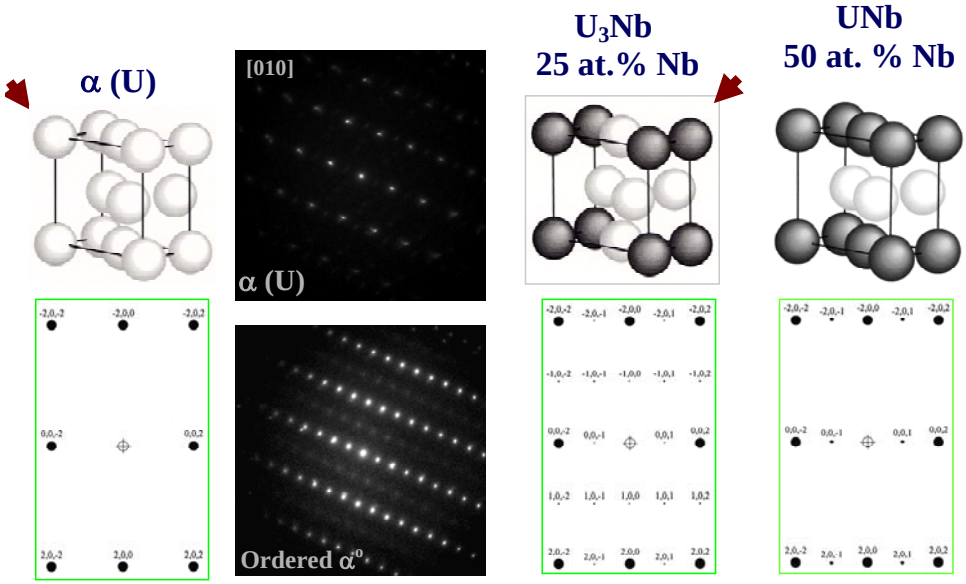

Fig. 9: The identification of Nb-depleted α phase and Nb-enriched U_3Nb ordered phase formed during accelerative aging of NA alloy at 200°C for 96 hours. TEM images and diffraction patterns (a) viewing from the [010]-zone; (c) a comparison between the observed [010]-zone diffraction patterns and the simulated [010]-zone patterns for the α (U), U_3Nb, and UNb phases.

Conclusions

Aging mechanisms and phase stability of water-quenched (WQ) U-6wt%Nb alloy artificial aging at 200°C, natural aging at ambient temperatures for 15 years, and natural aging followed by accelerative aging at 200°C have been investigated. The results show that: 1) Age hardening/softening phenomenon is observed from the artificially aged alloy, which can be rationalized by the occurrence of spinodal decomposition (i.e., the fine-scale of Nb segregation). 2) A chemical modulation along the [001] direction with a wavelength of ~3 nm is formed as a result of the spinodal decomposition. 3) An order-disorder transformation is found within the 15-yr naturally aged alloy based upon the observation of antiphase boundaries (APBs), which can be rationalized by the occurrence of an atomic-scale spinodal ordering along the [001] direction. 4) New chemically ordered U_3Nb phase is found to form within the 15-yr naturally aged (NA) alloy after accelerative aging at 200°C, which results in the occurrence of precipitation hardening.

Acknowledgements

This work was performed under the auspices of the U. S. Department of Energy by the University of California, Lawrence Livermore National Laboratory under Contract No. W-7405-Eng-48. The authors gratefully acknowledge Bob McKoon, Anne Sunwoo, and T. C. Sun for their contribution to the heat treatment of the U6Nb alloy, Cheng Saw and Octavio Cervantes for the X-ray diffraction analysis, Bob Vallier and Vicki Mason-Reed for the microhardness measurement, and Rick Gross and Jessee Welch for the preparation of TEM foils.

References

1. Vandermeer, R.A., *Acta Metall*., **28** (1980), p. 383.
2. Eckelmeyer, K.H., Romig, A.D., and Weirick, L.J., *Met. Trans. A*, **15A** (1984), p. 1319.
3. Vandermeer, R.A., Ogle, J.C., and Northcutt, Jr., W.G., *Met. Trans. A*, **12A** (1981), p. 733.
4. Field R.D., Thoma D.J., Dunn, P.S., Brown D.W., Cady. C.M, *Phil. Mag. A*, **81** (2001), p. 1691.
5. Jackson, R.J., Miley, D. V., *Trans. ASM*, **61** (1968), p. 336.
6. Beverini, G., Edmonds, D.V., *Colloque De Physique*, Colloque **C8**, C8-429.
7. Cahn J.W., Trans. *TMS of AIME*, **242** (1968), p. 166.
8. Sato K.and Stobbs, W.M., *Phil. Mag. A*, **69** (1994), 349.
9. Butler E.P. and Thomas, G., *Acta Metall*., **18** (1970), 347.
10. J.W. Edington, Practical Electron Microscopy in Materials Science, Van Nostrand Reinhold, New York, 1976.